Next Materials 3 (2024) 100172

Contents lists available at ScienceDirect

Next Materials

journal homepage: www.sciencedirect.com/journal/next-materials

Research article

Development of photo-crosslinked poly(aspartic acid) fiber networks via electrospinning

Lauren De Grave [a], Katrien V. Bernaerts [b], Sandra Van Vlierberghe [a,*]

[a] Polymer Chemistry and Biomaterials Group (PBM), Centre of Macromolecular Chemistry, Department of Organic and Macromolecular Chemistry, Ghent University, Krijgslaan 281, Building S4-bis, Ghent 9000, Belgium
[b] Sustainable Polymer Synthesis group, Aachen-Maastricht Institute for Biobased Materials (AMIBM), Maastricht University, Brightlands Chemelot Campus, Urmonderbaan 22, Geleen 6167 RD, the Netherlands

ARTICLE INFO

Keywords:
Polysuccinimide
Poly(aspartic acid)
Electrospinning
Photo-crosslinking
Fiber networks

ABSTRACT

Poly(aspartic acid) (pAsp)-based fiber networks were developed via electrospinning and photo-crosslinking. Fiber networks hold the advantage that they exhibit a high surface-to-volume ratio, giving rise to a high water uptake and retention capacity, along with the ability to release moisture under desired circumstances (*e.g.* reduced relative humidity, mechanical pressure, *etc.*). Herein, polysuccinimide (PSI), the precursor of pAsp, was modified with 5-norbornene-2-methylamine to obtain crosslinkable norbornene-modified PSI (PSI-NB) with two different degrees of substitution, *i.e.* 19% and 46%. These derivatives were electrospun into thin uniform fibers after optimization of the processing parameters. The fiber sheets were crosslinked via a thiol-ene step-growth mechanism with three different thiol crosslinkers exploiting UV-A irradiation in the presence of TPO-L as photo-initiator. Using this strategy, fiber networks with diameters ranging between 1.27 ± 0.29 and 2.20 ± 1.05 μm were obtained, as visualized with scanning electron microscopy (SEM). Successful crosslinking was evidenced by a dissolution test in dimethylformamide and through X-ray photoelectron spectroscopy. Finally, the PSI-NB fiber networks were hydrolyzed to obtain pAsp-NB fiber networks by alkaline hydrolysis in a carbonate buffer solution, as confirmed by Fourier-transform infrared spectroscopy. The morphology of the fibers following hydrolysis was visualized by SEM and the average fiber diameters were calculated and compared to the diameters before hydrolysis, generally showing a diameter increase due to swelling of the fibers in aqueous solution. In conclusion, pAsp-based fiber networks were successfully developed and stabilized via photo-crosslinking.

1. Introduction

Electrospinning is a versatile, low-cost processing technique able to fabricate thin polymer fibers with diameters in the micro- and nanometer ranges [1]. It relies on the generation of electric charges on the surface of a polymer solution or melt by application of a high voltage between a nozzle and a collector plate, causing an ejection of a polymer jet once the accumulated charges overcome the surface tension, resulting in stretching into thin fibers [2–4]. Due to the small dimensions that can be obtained with electrospinning, electrospun fibers are characterized by a particularly high surface-to-volume ratio and interesting mechanical properties (Young's moduli up to 2.07 × 10^5 MPa, depending on the material type) [5], rendering fibrous structures useful for many applications, *e.g.* food packaging [6], energy-conversion materials like solar cells and batteries [7,8], materials for filtration [9], pharmaceuticals and drug delivery [10,11], cosmetic applications and wound dressings [12,13]. Furthermore, electrospun fibrous structures strongly resemble the human extracellular matrix, making them highly useful in the field of tissue engineering [14–17]. However, for many of the above-mentioned applications, crosslinking of the fibers is required in order to retain their integrity in a medium and protect them from dissolving, which would result in loss of structure and consequently also loss of the properties [18]. Crosslinking is generally realized during electrospinning (*i.e.* reactive electrospinning) [19–21] or via the modification of polymers with crosslinkable side-groups followed by post-electrospinning crosslinking, including exposure of the crosslinkable electrospun fibers to UV light [22,23], heat [24] or γ-irradiation [25].

A wide range of polymers have been processed via electrospinning, both synthetic and natural, to obtain fibrous hydrogel structures, for

* Corresponding author.
E-mail address: Sandra.VanVlierberghe@UGent.be (S. Van Vlierberghe).

https://doi.org/10.1016/j.nxmate.2024.100172
Received 4 September 2023; Received in revised form 5 February 2024; Accepted 3 March 2024
Available online 6 March 2024

example collagen [26], gelatin [27,28], alginate [29], poly(oxazoline)s [30,31], acrylate-endcapped polyurethanes [13,32,33] and poly(acrylic acid) [34]. Collagen, gelatin and alginate are natural polymers exhibiting excellent biocompatibility and biodegradability. As a result, they are extremely useful for the preparation of fibrous membranes serving biomedical applications, but they suffer from issues in terms of reproducibility and limited freedom regarding modification strategies [35]. Poly(oxazoline)s are biocompatible synthetic polymers, with hydrophilic or hydrophobic properties depending on their side chain, which are synthesized in a controlled manner via cationic ring-opening polymerization [36]. The main advantage associated with acrylate-endcapped polyurethanes encompasses their solid-state photo-crosslinkability, in addition to their hydrophilicity and biocompatibility. However, these polymers also have limitations in terms of introducing functional side-groups [13]. Finally, poly(acrylic acid) is a synthetic polymer with a particularly high water absorption capacity as a result of its anionic nature, but it is based on fossil raw materials and it is also not biodegradable [37].

One type of polymers which have been emerging in recent years for fiber fabrication are poly(amino acid)s [38,39]. These synthetic polymers consist of amino acids, which are the building blocks constituting proteins and are therefore intrinsically biocompatible [40]. One of these is poly(aspartic acid) (pAsp), which is a water-soluble polyanionic polymer with excellent biocompatibility, biodegradability and properties similar to poly(acrylic acid). Therefore it has been considered as a sustainable alternative thereof [41,42]. When crosslinked, pAsp hydrogels can be made which exhibit a high water absorption capacity due to the high abundancy of carboxylic acid groups present in their chemical structure [43]. pAsp can be obtained by hydrolysis of its precursor polysuccinimide (PSI), which is synthesized through polycondensation of aspartic acid or by a reaction of maleic anhydride. Since PSI consists of reactive succinimide groups, modified pAsp can be easily synthesized by reaction of PSI with virtually any functional primary amine under mild reaction conditions followed by hydrolysis of the remaining succinimide units, providing a widely accessible range of modified pAsp derivatives [44]. pAsp-based fibrous materials hold great potential for use in biomedical (*e.g.* drug delivery [45,46], wound healing [47] and tissue engineering [20,48]) as well as sensing [49,50] applications. In addition to the high surface-to-volume ratio, surface area and porosity, which are characteristic for fibrous structures obtained via electrospinning [51], these applications can also greatly benefit from the hydrophilicity and anionic nature of the pAsp backbone [39,52,53]. As a result of their intrinsic hydrophilicity, pAsp-based fibrous networks show a high water uptake/retention capacity, rendering them promising for several applications, *e.g.* wound dressings and hydrating face masks [39,54]. Moreover, due to the possibility to introduce various functional side-groups in pAsp, electrospun fibrous pAsp networks can be highly tailored towards the desired application, for example to introduce affinity towards drugs or additives to create therapeutic wound dressings and skin care masks [54,55]. However, waterborne electrospinning of pAsp has not yet been described in literature and electrospinning from aqueous solutions is generally challenging due to the high boiling point of water [56]. Therefore, pAsp-based fibrous materials can be obtained by electrospinning of (modified) PSI, crosslinking and subsequent hydrolysis of the PSI fiber meshes. Crosslinking of PSI fibers is either done via reactive electrospinning or via post-electrospinning crosslinking. Reactive electrospinning of PSI can be done by electrospinning of modified PSI (*e.g.* with cysteamine) and spontaneous crosslinking of the fibers when they are emerging from the Taylor cone upon exposure to a trigger (*e.g.* exposure to air or UV light) [20,48,57] or via co-axial electrospinning when separate solutions of PSI and the crosslinker are electrospun and react by coming into contact with each other when leaving the needle [21]. Crosslinking via a post-electrospinning method on the other hand usually involves electrospinning of unmodified PSI and treatment with a solution containing a diamine to modify and crosslink the fibers [49,50,58–60]. Another possible post-electrospinning crosslinking method encompasses plasma treatment of electrospun allylamine-modified PSI [18].

Herein, we report the fabrication of fibers from PSI modified with norbornene side-groups followed by thiol-norbornene crosslinking upon UV irradiation, which is, to the best of our knowledge, the first report on photo-crosslinkable PSI fibrous materials. Using photo-induced crosslinking allows to tune the properties of the fiber networks by control over crosslinking density via the degree of modification of the electrospun fibers and variation of the thiol crosslinker used, in terms of spacer length, functionality and chemical structure. The parameters for electrospinning were optimized to obtain uniform, thin fibers which were investigated via scanning electron microscopy (SEM) and the fiber diameter distribution was calculated. The fibers were crosslinked with three structurally different thiol crosslinkers, as evidenced by a dissolution test and X-ray photoelectron spectroscopy (XPS). The crosslinked PSI-based fiber networks were converted into pAsp-based fiber networks through hydrolysis in an alkaline buffer solution, as shown by Fourier-transform infrared (FTIR) spectroscopy, and the influence of hydrolysis and the crosslinker used on the fiber morphology and diameter was investigated.

2. Materials and methods

2.1. Materials

DL-dithiothreitol (DTT, 97.0%), 2,2'-(ethylenedioxy)-diethanethiol (EDDET, 95.0%), trimethylolpropane tris(3-mercaptopropionate) (TMTMP, ≥ 95.0%), sodium bicarbonate ($NaHCO_3$, ACS reagent, ≥ 99.7%) and poly(ethylene glycol) (PEG, $M_v \sim 1{,}000{,}000$ g mol^{-1}) were purchased from Sigma-Aldrich. Sodium carbonate (Na_2CO_3, anhydrous, 99.5%) was acquired from Acros Organics. 5-Norbornene-2-methylamine (NB-NH_2, mixture of isomers, > 98.0%) was acquired from TCI Europe. Disinfectol (C_2H_5OH denaturated with 3% diethylether) was purchased from Chemlab. N,N-dimethylformamide (DMF, > 99.9%) was purchased from VWR. Ethyl acetate was supplied by UnivarSolutions. Ethyl (2,4,6-trimethylbenzoyl) phenylphosphinate (TPO-L) was supplied by SpeedCure. Deuterated dimethylsulfoxide (d_6-DMSO, 99.8% D) was obtained from Eurisotop. All chemicals were used as received. Polysuccinimide (PSI) was prepared according to a procedure described previously [61]. Double distilled water was used for the preparation of aqueous solutions (Merck Synergy UV, Millipore Milli-Q gradient, ρ = 18.2 MΩ cm at 25 °C).

2.2. Synthesis of norbornene-modified polysuccinimide (PSI-NB)

Synthesis of PSI-NB was performed according to our previously established procedure [61,62]. In brief, PSI (M_n = 13,400 g mol^{-1}, Đ = 4.1) was dissolved in DMF (10 w/v%) at 60 °C. After complete dissolution, NB-NH_2 was added to the PSI solution. A degree of substitution (DS) of 20% and 50% was targeted for the final norbornene-modified polysuccinimide (PSI-NB) by adding 0.20 eq. and 0.50 eq. (with respect to the amount of succinimide units in the starting material) of NB-NH_2, respectively. The reaction mixture was degassed 3 times and the reaction was continued for 24 h at 60 °C. The reaction mixture was precipitated in a 10-fold excess ethyl acetate, filtered, washed 3 times with ethyl acetate and dried under reduced pressure at 50 °C for 48 h.

2.3. Electrospinning of PSI-NB

Electrospun fibers were obtained using an in-house developed electrospinning set-up [22]. The set-up consisted of a high voltage source (Glassman high voltage DC power EL series), a collector plate and a syringe pump (ProSense B.V. NE-300) in a closed chamber with dehumidifier to decrease the relative humidity (RH) (Figure S1, **SI**). Electrospinning was performed at room temperature (21.5 ± 1.5 °C) and the

relative humidity (RH) in the chamber was on average 32%. Solutions were prepared containing 30 wt% PSI-NB precursor in DMF and 0.5 – 1 wt% PEG (1×10^6 g mol^{-1}) to ensure sufficient chain entanglements for electrospinning. The following parameters were varied in the electrospinning set-up: voltage (10 – 20 kV), needle diameter (18 – 21 gauge), flow rate (0.2 – 1.0 mL h^{-1}) and needle-to-collector distance (15 – 25 cm). The optimized electrospinning solution and parameters used to prepare fibrous samples for crosslinking and hydrolysis were: 30 wt% PSI-NB containing 0.5 wt% PEG (1×10^6 g mol^{-1}) in DMF, 15 kV voltage, 18 gauge needle diameter, 0.6 mL h^{-1} flow rate and 25 cm needle-to-collector distance.

2.4. Crosslinking of electrospun PSI-NB fibers

Crosslinking of the fibrous samples developed with the optimized electrospinning parameters was attempted with two bifunctional thiol crosslinkers (DTT and EDDET) and one trifunctional thiol crosslinker (TMTMP) (Fig. 1). Crosslinking solutions containing an excess of the thiol crosslinker and TPO-L photoinitiator in disinfectol were prepared, taking into account the DS of the electrospun PSI-NB fibers and the functionality of the crosslinker. The composition of the solutions used is presented in Table 1.

The samples ($15 \times 15 \times 0.025$ mm^3) were incubated in 5 mL of the crosslinking solutions for 24 h at room temperature. The solutions were degassed with N_2 gas for 1 min and sealed off from the air to limit the formation of disulfide bonds during the period of incubation. Afterwards, the incubated samples were irradiated from the top with UV-A light (365 nm, 10 mW cm^{-2}, UVP High Performance UV Transilluminator) for 2 h to induce crosslinking. The samples were covered with a UV transparent glass plate to avoid evaporation of the crosslinking solution. The samples were removed from the solution and washed with disinfectol to remove residual traces of the photo-initiator and crosslinker, followed by drying in the vacuum oven for 24 h at 60 °C to remove possible solvent remnants.

Table 1
Constitution of the solutions used for crosslinking of the PSI-NB fibrous samples.

Crosslinker	PSI-NB target DS 20%		PSI-NB target DS 50%	
	C_{TPO-L} (w/v %)	$C_{crosslinker}$ (w/v %)	C_{TPO-L} (w/v %)	$C_{crosslinker}$ (w/v %)
DTT	0.05	0.75	0.12	1.75
EDDET	0.05	0.75	0.12	1.75
TMTMP	0.05	0.50	0.12	1.15

Crosslinking of the fiber networks was evaluated by a dissolution test in DMF. The crosslinked fibrous samples and a non-crosslinked fibrous sample were incubated in DMF for 6 h, followed by washing with double distilled water and drying in the vacuum oven for 24 h at 60 °C. SEM was used to evaluate the morphology of the samples before and after the dissolution test.

2.5. Hydrolysis of PSI-NB fiber networks into pAsp-NB fiber networks

The crosslinked PSI-NB fiber networks were hydrolyzed to obtain crosslinked pAsp-NB fiber networks. The samples were placed in 3 mL of carbonate buffer (0.1 M, pH 10) for 6 h at room temperature to induce ring-opening of the succinimide rings in the fibrous structures. The samples were removed from the buffer solution and rinsed with double distilled water. The samples were dried overnight in the vacuum oven at 80 °C.

2.6. Characterization

2.6.1. Nuclear magnetic resonance (^{1}H NMR) spectroscopy

^{1}H NMR spectra were recorded on a 300 MHz Bruker Avance I Ultrashield spectrometer at room temperature with d_6-DMSO as solvent. Spectra were analyzed using MestReNova software.

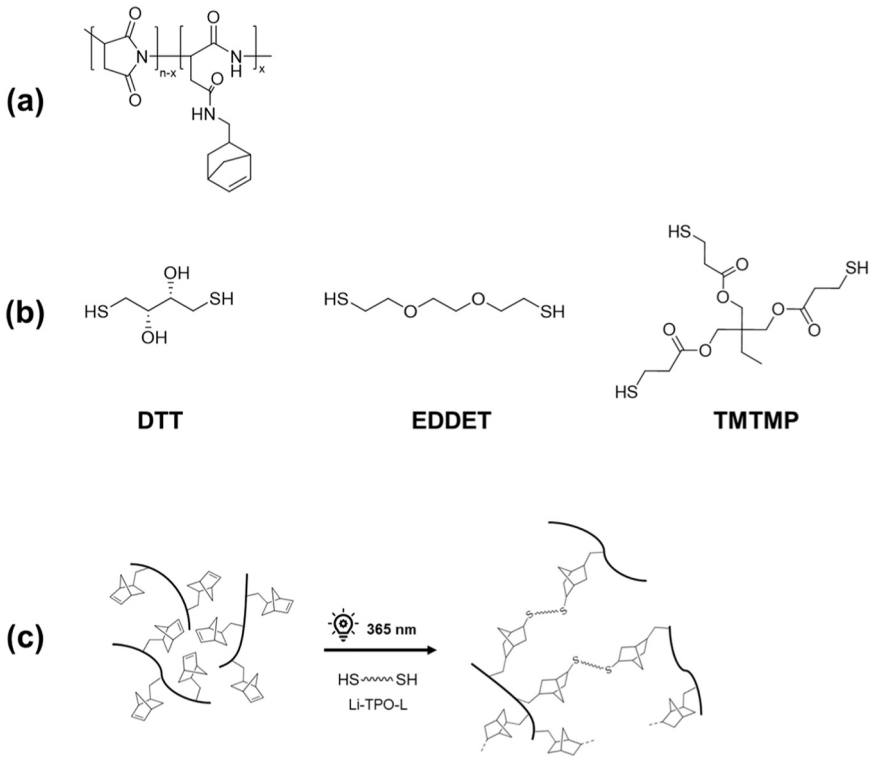

Fig. 1. (a) Chemical structure of PSI-NB, (b) chemical structures of the three thiol crosslinkers used to obtain PSI-NB fiber networks, i.e. DL-dithiothreitol (DTT), 2,2'-(ethylenedioxy)diethanethiol (EDDET) and trimethylolpropane tris(3-mercaptopropionate) (TMTMP), and (c) schematic representation of the thiol-norbornene crosslinking reaction.

2.6.2. Gel permeation chromatography (GPC)

GPC measurements were performed on a Waters Alliance e2696 Separations Module device coupled to one PSS GRAM analytical GPC precolumn (8.0 × 50 mm^2, 10 μm particle size), followed by one PSS GRAM analytical GPC column with molar mass range 100 – 10,000 g mol^{-1} (8.0 × 300 mm^2, 10 μm particle size) and two PSS GRAM analytical GPC columns with molar mass range 1000 – 1,000,000 g mol^{-1} (8.0 × 300 mm^2, 10 μm particle size) connected in sequence and exposed to a column temperature of 40 °C. Detection was based on a refractive index (RI) detector 2414 with temperature 35 °C. Molar masses were determined from the obtained retention times via an external calibration curve with ReadyCal-Kit PMMA standards (M_p = 800 – 2,200,000 g mol^{-1}). As eluent, DMF containing 0.035 mol L^{-1} LiCl was used at a flow rate of 1 mL min^{-1}. Samples were prepared by dissolving 5 mg of polymer in 1.5 mL of eluent.

2.6.3. Viscosity measurements

Prior to electrospinning, the viscosities of 30 wt% PSI-NB19 containing 0.5 wt% PEG and 30 wt% PSI-NB46 containing 0.5 wt% PEG were measured through rheology. Rheology measurements were performed on an Anton Paar Physica MCR 301 rheometer with parallel plate-plate geometry, with an upper plate diameter of 25 mm (PP25). All measurements were performed at 25 °C with a shear rate of 30 s^{-1}. 300 μL of the solution was injected between the parallel plates and a measuring gap of 0.300 mm was employed. The measurements were performed in triplicate for statistical relevance.

2.6.4. Scanning electron microscopy (SEM)

Fiber diameters and morphologies of the electrospun samples were visualized by SEM. Images were obtained with a Jeol JCM-700 benchtop SEM. The samples were dried prior to visualization in the vacuum oven at 60 °C for 24 h to remove all potential solvent remnants. Samples were attached to the sample stage with EM-Tec CT12 double-sided conductive carbon tape and sputter-coated with gold particles using an automatic Emitech Au Sputter Coater K550X with a RV3 two-stage rotary vane pump. Average fiber diameters and their standard deviations were determined using ImageJ software based on 100 measurements for each sample.

2.6.5. X-ray photoelectron spectroscopy (XPS)

Incorporation of the thiol crosslinkers in the fiber networks was studied by XPS. The PSI-NB fiber networks crosslinked with the three different thiol crosslinkers were compared to the non-crosslinked PSI-NB fiber mats. XPS was performed using an S-probe monochromatized XPS spectrometer from Surface Science Instruments (VG). The device had a monochromatic Al K_α X-ray source (1,486.6 eV), a take-off angle of 45°, a 10 kV voltage source and a 200 W power source. A flood gun and Ni grid were used for compensation of charging effects. The spectra were collected with a pass energy of 140.83 eV and energy steps of 0.160 eV. The base pressure of the measuring chamber was 1 × 10^{-7} Pa. The spot size was 250 × 1,000 μm^2. For each sample, two or three spots on the sample surface were measured and the relative atomic composition (at %) of the samples is given as the mean value of these measurements with their standard deviation. All spectra were analyzed using CasaXPS software.

2.6.6. Fourier-transform infrared spectroscopy (FTIR)

FTIR measurements were performed using a PerkinElmer Frontier FTIR spectrometer combined with a MKII Golden Gate Single Reflection Diamond ATR system from Specac. Spectra were recorded for a wavenumber range of 600 – 4,000 cm^{-1}. The spectra were analyzed with PerkinElmer Spectrum Analysis software.

2.6.7. Dynamic vapor sorption (DVS)

DVS measurements were executed to determine the moisture uptake capacity of the pAsp-NB fiber networks at different RH as well as sample hysteresis during desorption. The DVS device consists of a Cahn microbalance, a temperature-controlled housing and mass flow controllers to control the flow of wet and dry N_2 gas. This set-up allows to control both RH and temperature. The temperature was set at 20 °C for all measurements. 5 – 10 mg fibrous sample was placed in the sample pan. A first step at RH of 0% was established to start with completely dry material. Afterwards, the RH was increased in systematic steps of 10%, with a final step of 8%, until a RH of 98% was reached. Every subsequent step was initiated when the change in sample mass as a function of time was lower than 0.002 mg min^{-1}. After an equilibrium value was obtained at the highest RH, desorption was realized by decreasing the RH via the same systematic steps as the sorption process until complete desorption was realized.

2.6.8. Statistical analysis

The obtained fiber diameters and pore sizes are reported as their mean value with standard deviation. Significant differences in fiber diameters and pore sizes were identified by a one-way ANOVA test, followed by a Tukey post-hoc test when more than two samples were compared and a student's t-test when only two samples were compared. The tests were performed in SPSS Statistics 28 software and the level of significance was set at $p \leq 0.05$.

3. Results and discussion

3.1. Synthesis and characterization of PSI-NB

Photo-crosslinkable PSI was synthesized by modification of a PSI (M_n = 13,400 g mol^{-1}, Đ = 4.1, as determined via GPC in DMF containing 0.035 mol L^{-1} LiCl) precursor with a functional primary amine, namely NB-NH_2 (Figure S2, **SI**). Two PSI-NB derivatives with a different targeted DS (20% and 50%) were synthesized by adding 0.20 and 0.50 eq. NB-NH_2, with respect to the amount of succinimide units in the PSI. When adding 0.20 eq. NB-NH_2, PSI-NB with a DS of 19% was obtained with a yield of 63%, while when adding 0.50 eq., PSI-NB with a DS of 46% and a yield of 82% was obtained, which will be further referred to as PSI-NB19 and PSI-NB46, respectively. The obtained DS was calculated exploiting the relative integrations from the ^{1}H NMR spectra (Figure S3, **SI**). PSI-NB19 exhibited a number-average molar mass (M_n) of 10,200 g mol^{-1} and a dispersity (Đ) of 2.2 and PSI-NB46 had an M_n of 12,300 g mol^{-1} and a Đ = 1.9, as determined via GPC in DMF containing 0.035 mol L^{-1} LiCl (Figure S4, **SI**).

3.2. Electrospinning of PSI-NB

In order to produce PSI-NB based fibers which could be crosslinked and hydrolyzed, the parameters of the electrospinning process were optimized. The parameters were optimized for the PSI-NB19 derivative and afterwards also adopted for the PSI-NB46 derivative. The first parameter that was varied was the constitution of the polymer solution. Using a solvent with a moderate volatility (*e.g.* pure ethanol or mixtures thereof), which is generally beneficial for electrospinning as it results in a faster evaporation of the solvent upon deposition of the fibers [2,63], was not an option since the developed PSI-NB derivatives are only soluble in DMF and dimethyl sulfoxide (DMSO). Therefore, all solutions used for electrospinning were prepared in DMF. Solutions of PSI-NB19 in DMF with a concentration ranging from 20 to 50 wt% were prepared. The polymer concentration should not be too low as this leads to the formation of isolated droplets instead of a continuous flow when it leaves the needle, which is necessary to spin thin fibers, while a high concentration quickly leads to blockage of the needle [64]. However, electrospinning attempts of solutions of pure PSI-NB in DMF failed for all tested concentrations and electrospraying occurred instead, which entails the deposition of small particles from a polymer solution by fast evaporation of the solvent under the influence of the high voltage [65]. This process is related to electrospinning and uses a similar set-up, while

the occurrence of one versus the other is mainly dictated by the concentration of the solution and the molar mass of the polymer. When the concentration and molar mass are both high, the charged polymer jet originating from the Taylor cone is stabilized by chain entanglements and elongation into fibers takes place by whipping instability [66]. When the concentration and/or the molar mass are however too low, insufficient chain entanglements are present to stabilize the jet, causing the fibers to break which results in the formation of fine droplets instead [64,67]. Hence, the formation of particles instead of fibers indicated that the molar mass of the polymer used was not high enough to provide sufficient chain entanglements. An elegant way to solve this problem encompasses the addition of another polymer with high molar mass in small quantities, for example high-M_w PEG (1×10^6 g mol^{-1}) [13,22,29]. Therefore, 0.5 versus 1 wt% high-M_w PEG were added to a solution of PSI-NB19 with a moderate concentration (30 wt%) to induce more entanglements and to improve fiber formation.

The four other parameters that were varied in the set-up include the needle diameter, the distance between the needle and the collector plate, the flow rate of the polymer solution and the applied voltage. The needle diameters employed were 18 gauge (0.838 mm) and 21 gauge (0.495 mm). However, the use of a small needle diameter (21 gauge) led to blockage of the needle and an irregular polymer jet. Therefore, a needle diameter of 18 gauge was used for further optimization. Furthermore, the flow rate was varied between 0.3 and 0.6 mL h^{-1}, the needle-to-collector distance between 15 and 25 cm and the voltage between 10 and 20 kV. SEM images of the resulting electrospun fiber sheets are displayed in Fig. 2

When considering the SEM images, one can observe that rather uniform fibers with small diameters and a random deposition were obtained. For the solution containing 0.5 wt% PEG (Fig. 2**a-b**), the fiber diameter decreased when going from a flow rate of 0.3 – 0.6 mL h^{-1} at a needle-to-collector distance of 15 cm and a voltage of 10 kV (images A

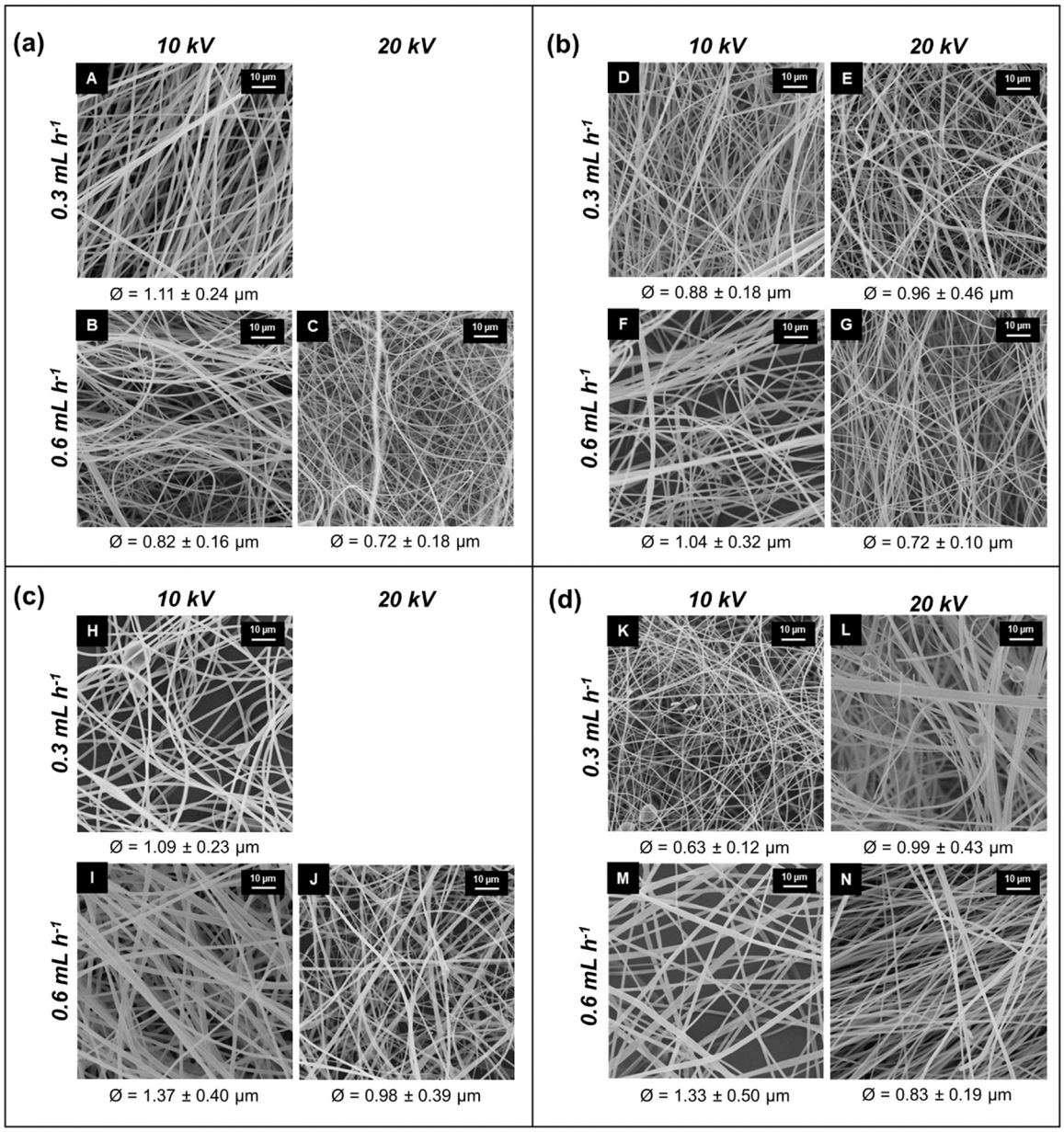

Fig. 2. SEM images of fibers obtained through electrospinning of a solution of 30 wt% PSI-NB19 with a 18 gauge needle exploiting (a) 0.5 wt% PEG (1×10^6 g mol^{-1}) and a needle-to-collector distance of 15 cm, (b) 0.5 wt% PEG (1×10^6 g mol^{-1}) and a needle-to-collector distance of 25 cm, (c) 1 wt% PEG (1×10^6 g mol^{-1}) and a needle-to-collector distance of 15 cm or (d) 1 wt% PEG (1×10^6 g mol^{-1}) and a needle-to-collector distance of 25 cm in DMF and through variation of flow rate and voltage. The average fiber diameter is provided below each image.

and B). The latter is not in agreement with many literature reports, as the fiber diameter generally increases with increasing flow rate, since a higher flow rate results in a higher deposited volume and an increased fiber diameter [68,69]. However, other literature reports also showed that upon exceeding a critical flow rate threshold, again a decrease of the fiber diameter occurred [70,71]. At a distance of 25 cm, the fiber diameter showed the expected trend at 10 kV and the fiber diameter increased with increasing flow rate (images D and F), while the difference in fiber diameter with variation of flow rate was not significant ($p > 0.05$) at a voltage of 20 kV (images E and G). For a flow rate of 0.6 mL h^{-1} and a distance 15 cm, there were no significant differences in average fiber diameter when going from 10 to 20 kV (images B and C). For a distance of 25 cm and a constant flow rate of 0.3 mL h^{-1}, there was no significant difference in fiber diameter when increasing the voltage (images D and E), while it did decrease with increasing voltage for a flow rate of 0.6 mL h^{-1} (images F and G). Literature showed that the fiber diameter generally decreases with increasing voltage, which is a result of the electrostatic repulsive forces on the polymer surface, which results in a higher tensile force on the polymer jet and hence a reduction in fiber diameter. Considering a constant flow rate of 0.3 mL h^{-1} and constant voltage of 10 kV, the fiber diameter also decreased with increasing needle-to-collector distance (images A and D), while this was the other way around for a flow rate of 0.6 mL h^{-1} and a voltage of 10 kV (images B and F). At a higher voltage, the fiber diameter was independent of the distance (images C and G). Generally, the fiber diameter decreases with increasing needle-to-collector distance, as the solvent has more time to evaporate from the polymer solution jet and full extension of the fiber thread can be achieved [71]. For the solution containing 1 wt% PEG (Fig. 2**c-d**), fibers with defects (droplets and irregularities) were formed when electrospun at a flow rate of 0.3 mL h^{-1} irrespective of the voltage and distance (images H, K and L). Therefore, these conditions were not considered as no uniform fibers could be produced. For a flow rate of 0.6 mL h^{-1}, a decrease in average fiber diameter with increasing voltage was observed, both for a needle-to-collector distance of 15 cm (images I and J) and 25 cm (images M and N). The fiber diameter was independent of the needle-to-collector distance when considering a constant flow rate and voltage (images I and M; J and N). In Fig. 2, no images are presented for electrospinning at a flow rate of 0.3 mL h^{-1}, a distance of 15 cm and a voltage of 20 kV, both for 0.5 and 1 wt% PEG. For the solution containing 1 wt% PEG, no electrospinning was possible exploiting the conditions mentioned. For the solution containing 0.5 wt% PEG, fibers were deposited on the collector plate, but also thick threads of the polymer solution jet were deposited since the solvent was not completely evaporated. As the sample contained a lot of solvent remnants, no SEM pictures were recorded, but optical microscopy images show thin fibers connected by large clots of polymer solution (Figure S5, **SI**).

Furthermore, the fiber diameter distribution of all samples obtained via electrospinning and resulting from a variation of the electrospinning parameters was determined. Fig. 3 shows the fiber diameter distribution of the samples which were electrospun with a needle-to-collector distance of 25 cm and a voltage of 20 kV. For a solution of 30 wt% PSI-NB19 containing 0.5 wt% PEG (Fig. 3**a-b**), a non-uniform fiber distribution was obtained for a flow rate of 0.3 mL h^{-1} with fiber diameters ranging between 0.30 and 2.40 μm. For a flow rate of 0.6 mL h^{-1} on the other hand, a uniform distribution was observed with all fiber diameters ranging between 0.50 and 1.10 μm and the main fraction within 0.70 – 0.80 μm (Fig. 2**a**, image G). For a solution of 30 wt% PSI-NB19 containing 1 wt% PEG (Fig. 3**c-d**), broader fiber diameter distributions could be observed at both flow rates applied. However, similar to the solutions containing 0.5 wt% PEG, the fiber diameter became more narrow with increasing flow rate. For a flow rate of 0.6 mL h^{-1}, the fiber diameter distribution was relatively narrow with all fiber diameters being situated between 0.50 and 1.40 μm. The fiber diameter distributions for the other conditions are depicted in the supplementary information (Figure S6).

Based on the results obtained from SEM and the calculated fiber diameter distributions, fiber sheets for crosslinking were prepared using the following electrospinning conditions: 30 wt% solution PSI-NB (DS 19% or 46%) containing 0.5 wt% PEG (1×10^6 g mol^{-1}), 18 gauge needle diameter, 0.6 mL h^{-1} flow rate, 25 cm needle-to-collector distance and 15 kV voltage. Viscosity measurements of the employed solutions prior to electrospinning provided values of 2.01 ± 0.21 Pa s and 1.4 ± 0.25 Pa s (25 °C, 30 s^{-1} shear rate) for the 30 wt% PSI-NB19 + 0.5 wt% PEG and 30 wt% PSI-NB46 + 0.5 wt% PEG solution, respectively. Both viscosities observed are within the range of values reported earlier for electrospinning of PSI-based solutions in literature [20,46].

3.3. Crosslinking of electrospun PSI-NB fibers to obtain PSI-NB fiber networks

The electrospun PSI-NB fiber sheets were crosslinked with three types of thiol crosslinkers to obtain PSI-NB fiber networks (Fig. 1). The thiol crosslinkers were selected based on their structural differences in order to study their effect on the fiber morphology following crosslinking. DTT is a bifunctional thiol with a relatively short spacer, EDDET is a bifunctional thiol with a slightly longer spacer and TMTMP is a trifunctional star-shaped thiol. Crosslinking was realized by incubating the PSI-NB fiber sheets in a solution with excess of the thiol crosslinker and the TPO-L photo-initiator in disinfectol for 24 h, followed by irradiation with UV-A light for 2 h. The incubation period of 24 h was chosen to allow the crosslinking solution to penetrate into the fibers and allow crosslinking also in their core. Furthermore, it was also investigated whether the fibers could be crosslinked in the "dry state" by treatment with UV after removal of the crosslinking solution instead of in the solution. Investigation of the fiber morphology with optical

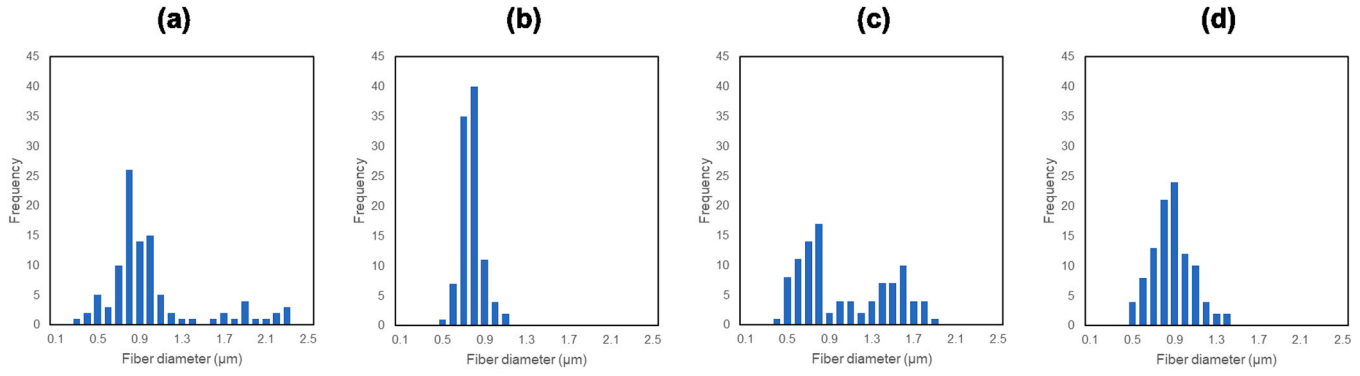

Fig. 3. Distribution of the diameters of fibers obtained via electrospinning with a 18 gauge needle (0.838 mm), a needle-to-collector distance of 25 cm and a voltage of 20 kV exploiting a solution of 30 wt% PSI-NB19 containing (a) 0.5 wt% PEG and a 0.3 mL h^{-1} flow rate, (b) 0.5 wt% PEG and a 0.6 mL h^{-1} flow rate, (c) 1 wt% PEG and a 0.3 mL h^{-1} flow rate or (d) 1 wt% PEG and a 0.6 mL h^{-1} flow rate.

microscopy prior to SEM measurements showed a superior retention of the fiber morphology upon UV treatment in the presence of the crosslinking solution compared to in the absence of the solution, particularly for the crosslinked PSI-NB46 fibers (Figure S7**, SI**). Hence, UV treatment in solution was selected to retain the fiber morphology and to ensure maximum availability of the crosslinker and photo-initiator during the crosslinking process.

To prove successful crosslinking, the obtained PSI-NB fiber networks were subjected to a dissolution test in DMF, which is an excellent solvent for PSI and PSI derivatives [60]. The non-crosslinked fiber sheets of both PSI-NB19 and PSI-NB46 immediately dissolved when they were immersed in DMF, while the crosslinked fiber networks remained intact, indicating the presence of crosslinks that maintained the fiber structure and protected them from dissolving. SEM was used to study the effect of incubation in DMF on the fiber morphology and fiber diameter. Fig. 4 shows SEM images of PSI-NB19 and PSI-NB46 fibers crosslinked with DTT before and after exposure to DMF. For both crosslinked PSI-NB19 and PSI-NB46, no visual changes in fiber morphology were apparent following exposure to DMF and the fibers could still be distinguished. The average fiber diameters observed were not significantly different ($p > 0.05$) before (1.93 ± 0.72 μm for PSI-NB19 + DTT and 1.48 ± 0.34 μm for PSI-NB46 + DTT) and after (1.89 ± 0.79 μm for PSI-NB19 + DTT and 1.41 ± 0.24 μm for PSI-NB46 + DTT) the dissolution test.

The presence of crosslinks was further evidenced by XPS measurements. The relative atomic composition in percentages (at%) of each sample was calculated as the average value of the elements obtained by measurement of two or three spots on the surface of each sample. The calculated relative at% for each sample are summarized in Table 2 and one representative spectrum of each sample can be found in the supplementary information (Figure S9). For all samples where a crosslinker was used, two signals for sulfur (164 eV for S 2p and 229 eV for S 2 s) could be identified in the spectra, which indicated the presence of this element in the fibrous structures and hence the incorporation of the thiol crosslinker. Only for PSI-NB19 + DTT, no S was detected, indicating that the at% was probably below the detection limit of XPS, which is 0.1 – 1 at% for nearly all elements [72]. For PSI-NB46 + DTT on the other hand, the presence of S was clearly detected. When comparing the samples of PSI-NB19 and PSI-NB46 crosslinked with EDDET, one can observe that a significantly ($p < 0.05$) higher at% of S was obtained for the higher DS, as a higher content of crosslinker was used for higher DS PSI-NB. For PSI-NB46 + TMTMP, the at% of S was not significantly ($p > 0.05$) different from the at% obtained for PSI-NB19 + TMTMP. However, XPS is a surface analysis technique with a penetration depth of ~10 nm, hence only conclusions can be made regarding the composition of the surface of the samples and not on the bulk of the material.

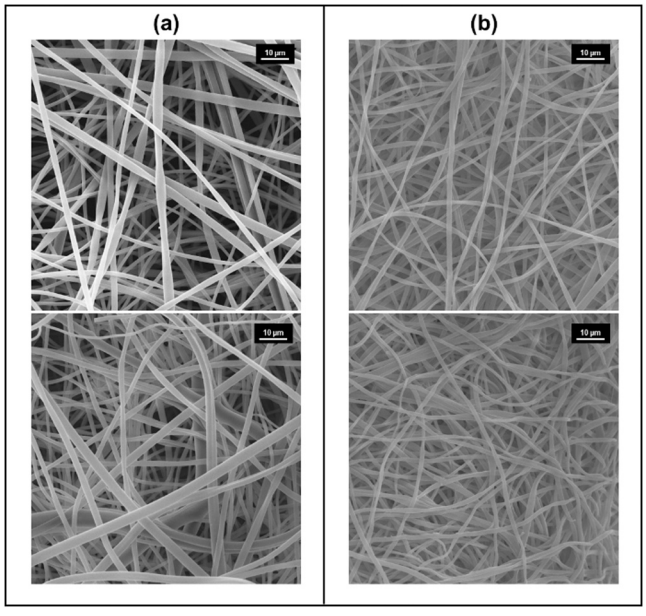

Fig. 4. Comparison of the fiber morphology of (a) PSI-NB19 and (b) PSI-NB46 fiber networks crosslinked with DTT before (top) and after (bottom) the dissolution test in DMF.

Table 2
Average at% with standard deviation of each sample calculated based on XPS spectra.

Sample	C 1 s (%)	N 1 s (%)	O 1 s (%)	S 2p (%)
PSI-NB19	66.3 ± 1.3	9.2 ± 1.9	24.5 ± 0.7	
PSI-NB19 + DTT	66.8 ± 0.2	9.4 ± 0.9	23.8 ± 0.7	
PSI-NB19 + EDDET	65.4 ± 2.3	7.4 ± 1.9	23.5 ± 0.6	3.7 ± 0.5
PSI-NB19 + TMTMP	66.4 ± 0.5	8.7 ± 0.3	21.6 ± 1.0	3.3 ± 0.2
PSI-NB46	67.9 ± 1.8	10.8 ± 0.2	21.3 ± 1.6	
PSI-NB46 + DTT	65.1 ± 0.1	6.3 ± 1.6	23.2 ± 0.4	5.5 ± 1.2
PSI-NB46 + EDDET	64.6 ± 0.7	1.9 ± 0.2	24.0 ± 0.5	9.6 ± 0.3
PSI-NB46 + TMTMP	74.4 ± 1.6	1.6 ± 1.4	23.2 ± 1.0	0.8 ± 1.1

3.4. Hydrolysis of PSI-NB fiber networks into pAsp-NB fiber networks

Following incubation in the crosslinking solution and treatment with UV irradiation, the PSI-NB fiber networks were incubated in a carbonate buffer solution (0.1 M, pH 10) at room temperature for 6 h to induce alkaline hydrolysis of the remaining succinimide units in the PSI-NB fibers to convert them into aspartic acid units thereby obtaining pAsp-NB fibers. The method for hydrolysis of the fiber networks was based on previously reported procedures [18,20,60], but the buffer solution, time and temperature were optimized for the fibers described herein. The samples were still visible and kept their integrity after this incubation period, indicating that they were not soluble in the buffer solution and the crosslinks were strong enough to resist the swelling resulting from the conversion of PSI into pAsp. The color of the samples went from white to almost completely transparent and they exhibited a more gel-like appearance, indicating the conversion into a more hydrophilic structure that absorbed the aqueous buffer solution.

The conversion from PSI-NB fiber networks into pAsp-NB fiber networks was confirmed by FTIR spectroscopy (Fig. 5), as PSI and pAsp both have characteristic signals in their fingerprint region that allow to differentiate between them [44]. Before hydrolysis, a characteristic band was observed at 1390 cm^{-1} which originated from N-H bending and C-N stretching from the amide moieties. Furthermore, a strong peak at 1710 cm^{-1} and a smaller peak at 1790 cm^{-1} could be observed, which originated from the C═O stretching and an adjacent carbonyl coupling effect, indicating the presence of an imide ring structure. When considering the spectra of the PSI-NB46 fiber networks before crosslinking (Fig. 5**b**), the signal at 1650 cm^{-1} became more prominent while it was only visible as a "shoulder" signal of the peak at 1710 cm^{-1} in the spectra of PSI-NB19 fiber networks (Fig. 5**a**). This signal could be attributed to N-H bending which was stronger for PSI-NB46, as there were more NH entities present in the structure compared to PSI-NB19 due to the higher modification degree. When comparing with the spectra after hydrolysis, the most pronounced difference was the disappearance of the strong signals at 1710 cm^{-1} and 1790 cm^{-1}, indicating the absence of imides from PSI and the successful conversion into pAsp. Furthermore, an absorption band appeared at 1600 cm^{-1}, which was a result of the stronger N-H bending that originated from the higher abundancy of NH groups present in pAsp compared to PSI. However, only for PSI-NB46 crosslinked with TMTMP, the peak at 1710 cm^{-1} remained more prominent compared to the absorption band at 1600 cm^{-1} after hydrolysis, indicating that conversion to pAsp-NB46 upon incubation for 6 h in the buffer solution was not complete. This can be a result of the higher crosslinking density of the sample, causing less swelling of the network and consequently less hydrolysis. In an attempt

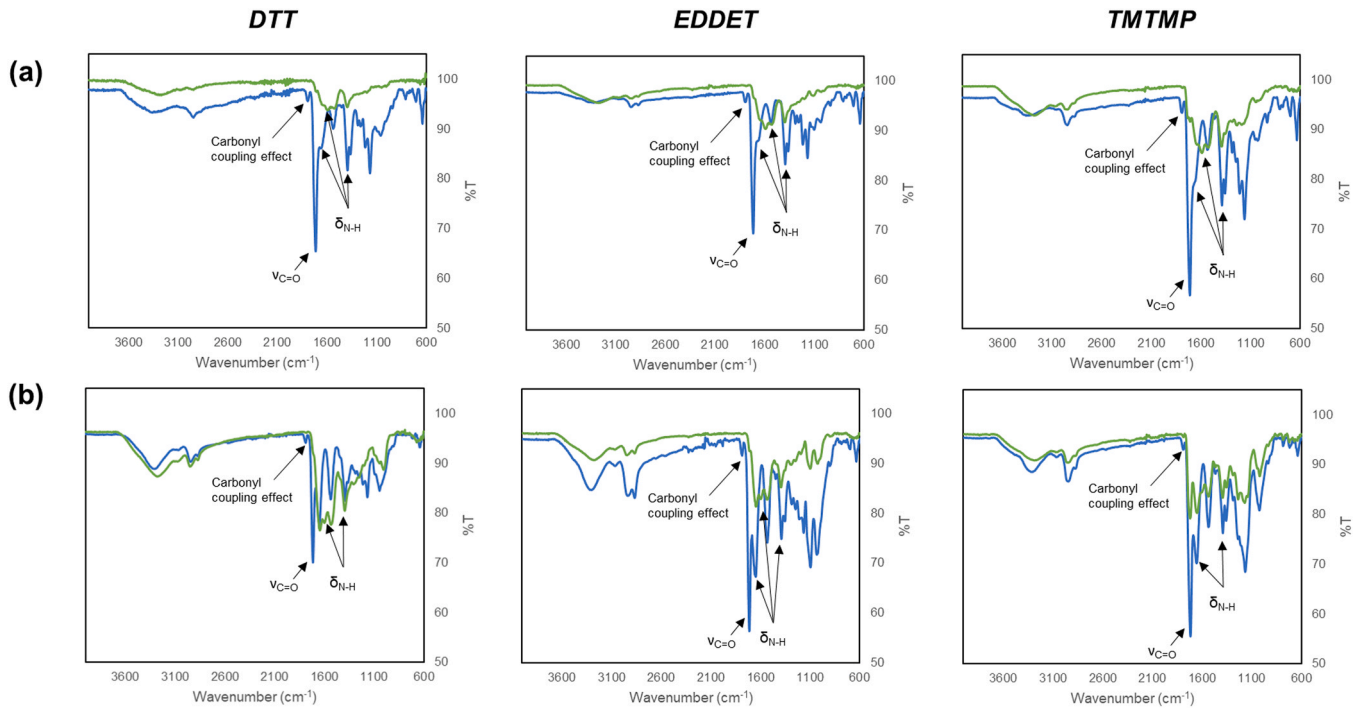

Fig. 5. FTIR spectra of the fibrous networks before (blue line) and after (green line) hydrolysis of (a) PSI-NB19 and (b) PSI-NB46 crosslinked with DTT, EDDET and TMTMP.

to realize complete hydrolysis of PSI-NB46 + TMTMP fibers, the time of incubation in the buffer solution was prolonged with several hours up to 3 days (**Section 4 , SI**). However, when considering the spectra obtained of the samples after different time points, it is clear that the characteristic PSI peak at 1710 cm^{-1} never completely disappeared, even after 72 h (Figure S10**, SI**). Therefore, for further discussion of the results, the time of incubation in the buffer solution was kept at 6 h to be able to compare the obtained fiber network with the others and because exposure to an alkaline medium for a long period of time can result in degradation of the peptide bonds [73], which would disintegrate the fiber network.

SEM measurements were executed on the PSI-NB fiber networks and the pAsp-NB fiber networks after drying in the vacuum oven to compare the morphology and average fiber diameters before and after hydrolysis (Fig. 6). A first observation that can be made is that all fiber networks, irrespective of the DS or the crosslinker used, retained their fibrous structure, which shows that our strategy outperforms multiple previously reported strategies to create pAsp-based fiber networks [18, 74–76]. Furthermore, a morphological change could be observed for the fiber networks following hydrolysis, as they exhibited a more swollen and dense appearance. Only for PSI-NB46 + TMTMP, the morphological change was limited, which can be explained by the hydrolysis that was not completed and therefore resulted in more resemblance in chemical structure between the networks before and after hydrolysis. SEM images at higher magnification are provided in the supporting information (Figure S11). The average fiber diameters before and after hydrolysis were calculated and are summarized in Table 3. In general, the fiber diameter increased following hydrolysis. This increase can be attributed to the conversion of PSI into pAsp in the fiber structure, leading to the formation of hydrogel fibers that take up aqueous solutions and swell. For PSI-NB19 + DTT, PSI-NB46 + DTT and PSI-NB19 + EDDET, the differences in diameter before and after were, however, not significant. For PSI-NB46 + EDDET and PSI-NB46 + TMTMP, moderate increases in fiber diameter of 17% and 27%, respectively, were observed upon hydrolysis. For PSI-NB19 + TMTMP, a more significant increase in fiber diameter (79%) was observed, which can be attributed to the lower DS of the fibers, leading to a less dense network architecture and hence a higher swelling [77]. Furthermore, when examining the SEM images in greater detail, the fusion of some of the fibers and cord-like structures of several fibers running in parallel can be observed following hydrolysis, in particular for PSI-NB19 + TMTMP, which also resulted in the larger fiber diameters observed [60]. The fiber diameter distribution was in general more uniform for the PSI-NB46 fiber networks compared to the PSI-NB19 fiber networks, both before and after hydrolysis and for all crosslinkers, which was reflected by the smaller standard deviations of the average diameters.

Visually, a reduction in average pore size upon hydrolysis of the fibrous networks could be observed. The average pore sizes were calculated exploiting the SEM images and are also included in Table 3. The calculated average pore sizes (*i.e.* distance between fibers) were used to get an indication regarding the change in porosity upon hydrolysis. For both DS, a significant decrease ($p \leq 0.05$) in average pore size was observed for the fibrous networks crosslinked with DTT and EDDET. For PSI-NB19 + DTT and PSI-NB19 + EDDET, the pore sizes decreased with 55% and 24%, respectively. For PSI-NB46 + DTT and PSI-NB46 + EDDET, the average pore sizes showed a decrease of 18%. The larger reduction observed for the samples with the lower DS was expected, when considering the lower network density which results in a higher swelling [77]. The differences in pore size before and after hydrolysis were not significant ($p > 0.05$) for PSI-NB19 + TMTMP and PSI-NB46 + TMTMP. The observed decrease in average pore size and increase in average fiber diameter resulted in a more densely packed membrane following hydrolysis. The pore sizes and pore size reductions observed upon hydrolysis from PSI- to pAsp-based fiber networks are in line with previous reports from literature, showing mean pore sizes in the range of 1 – 8 μm [59,78].

The moisture uptake capacity of the pAsp-NB fibrous networks with different DS and thiol crosslinkers was determined via DVS measurements as a function of RH. Two isotherms, representing the sorption and desorption of moisture, were obtained. In Table 4, the moisture uptake at low, medium and high RH are displayed. For the pAsp-NB19 crosslinked fiber networks, the moisture uptake capacity showed similar values irrespective of the crosslinker type applied. All networks showed an uptake capacity > 100% their own mass at high RH, indicating that

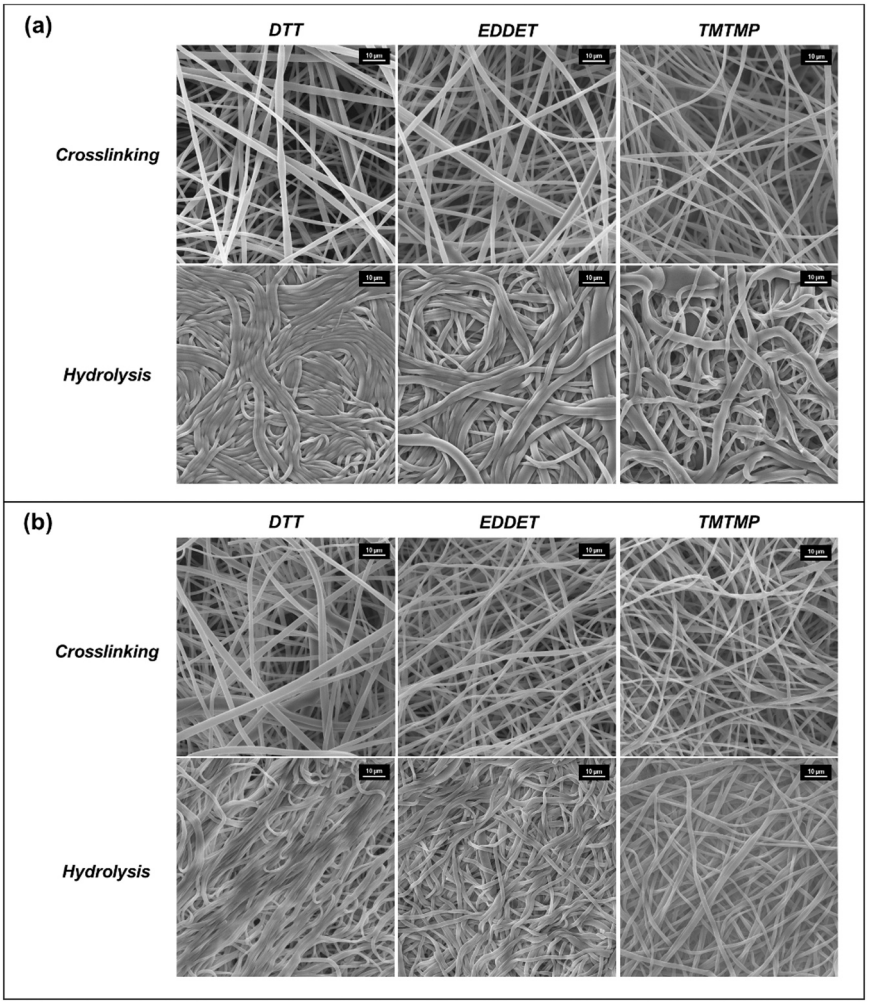

Fig. 6. SEM images of the PSI-NB fiber networks after crosslinking of (a) PSI-NB19 and (b) PSI-NB46 and after hydrolysis in the carbonate buffer solution (0.1 M, pH 10) to obtain pAsp-NB fiber networks.

Table 3
Average fiber diameters and pore sizes of the fiber networks crosslinked with the different thiol crosslinkers before and after hydrolysis. The values obtained after hydrolysis which are significantly different ($p \leq 0.05$) from the values before hydrolysis are marked with an asterisk (*).

DS (%)	Crosslinker	Average fiber diameter		Average pore size		
		Before hydrolysis (μm)	After hydrolysis (μm)	Before hydrolysis (μm)	After hydrolysis (μm)	Reduction (%)
19	DTT	1.93 ± 0.72	1.82 ± 0.55	2.46 ± 0.97	1.11 ± 0.41*	54.7
	EDDET	2.20 ± 1.05	2.60 ± 1.16	2.41 ± 0.86	1.84 ± 0.67*	23.8
	TMTMP	1.49 ± 0.48	2.67 ± 1.17*	2.89 ± 1.12	2.61 ± 0.97	10.0
46	DTT	1.48 ± 0.34	1.43 ± 0.40	2.22 ± 0.76	1.81 ± 0.74*	18.1
	EDDET	1.39 ± 0.26	1.63 ± 0.40*	2.03 ± 0.74	1.67 ± 0.49*	17.8
	TMTMP	1.27 ± 0.29	1.62 ± 0.41*	2.21 ± 0.75	2.02 ± 0.51	8.7

Table 4
Moisture uptake (%) of the pAsp-NB crosslinked fiber networks at 30%, 60% and 98% RH.

DS (%)	Crosslinker	Moisture uptake (%)		
		30% RH	60% RH	98% RH
19	DTT	6.6	16.9	115.3
	EDDET	6.5	15.3	104.5
	TMTMP	6.1	15.5	104.3
46	DTT	5.7	13.3	62.7
	EDDET	8.7	15.6	70.9
	TMTMP	7.2	11.6	33.5

the hydrogel fiber networks can absorb and retain high moisture amounts. For pAsp-NB46, the moisture uptake capacity at low and medium RH was independent of the crosslinker used and showed similar values to those obtained for pAsp-NB19. At high RH (98%), the moisture uptake showed a larger discrepancy depending on the crosslinker type. For DTT and EDDET, relatively high moisture uptake capacities of 62.7% and 70.9% were found, respectively. For TMTMP, the moisture uptake was only 33.5% at RH 98%, which can be explained by the incomplete hydrolysis of the network, resulting in a lower content of hydrophilic aspartic acid units. Furthermore, a limited hysteresis, which is defined as the difference between the sorption and desorption isotherm, was observed for the pAsp-NB19 networks (Figure S12**, SI**), indicating that the hydrogel fiber networks desorb most of the initially

absorbed moisture again at similar RH. For pAsp-NB46, a larger hysteresis was observed, at medium and high RH, especially for pAsp-NB46 + TMTMP. Hence, particularly the pAsp-NB19 fibrous hydrogel networks are promising to be used in applications which require high absorption and quantitative desorption of the absorbed moisture, for example to serve as wound dressings to absorb wound fluids or release therapeutic substances [79].

4. Conclusions

Herein, pAsp-based fibrous networks were developed by photo-crosslinking and hydrolysis of PSI-based electrospun fibers. PSI was first modified with NB resulting in DS values of 19% and 46%, in order to obtain photo-crosslinkable PSI. The effect of the electrospinning parameters on the average diameter and morphology of the fibers was investigated and the electrospinning process was optimized for PSI-NB with low DS in order to obtain uniform thin fibers. It was also shown that the addition of high-M_w PEG to PSI-NB was necessary to establish sufficient chain entanglements to make fiber sheets. The PSI-NB19 and PSI-NB46 fibers were crosslinked with three types of thiol crosslinkers, DTT, EDDET and TMTMP, and irradiation with UV light. The crosslinked fiber networks retained their structure when they were exposed to DMF, which is an excellent solvent for PSI-based materials, and the average fiber diameter remained constant (1.93 ± 0.72 μm before exposure vs. 1.89 ± 0.79 μm after exposure for PSI-NB19 + DTT) or decreased only slightly (1.48 ± 0.34 μm before exposure vs. 1.41 ± 0.24 μm after exposure for PSI-NB46 + DTT). Furthermore, the crosslinked PSI-based fiber networks were converted into pAsp-based fiber networks by incubation in a carbonate buffer (0.1 M, pH 10) for 6 h at room temperature. FTIR measurements showed successful conversion into pAsp-based fiber networks as the characteristic peaks for PSI in the spectrum at 1710 cm^{-1} and 1790 cm^{-1} disappeared and were replaced by an absorption band at 1600 cm^{-1}, which is characteristic for pAsp. Only for PSI-NB46 + TMTMP, no complete conversion could be obtained. SEM images of the samples before and after hydrolysis showed a clear change in morphology of the fibers, and the pAsp fibrous networks had a swollen appearance. Generally, the change in average fiber diameter before and after hydrolysis was dependent on the crosslinker used and the DS, indicating a difference in network density. For PSI-NB crosslinked with DTT, no increase in fiber diameter was observed, PSI-NB crosslinked with EDDET showed a slight increase while PSI-NB crosslinked with TMTMP showed a larger increase, especially for a DS of 19% (increase with 79%). Finally, the moisture uptake capacity of the fibrous hydrogel networks was assessed through DVS measurements, which evidenced that the networks resulting from low DS pAsp could take up > 100% its own mass in moisture at high RH, which was also released while showing limited hysteresis upon decreasing the RH.

In the current work, the possibility to fabricate PSI-based fiber networks through photo-crosslinking and hydrolysis into pAsp-based fiber networks was shown. These biobased fibrous networks with high water uptake/retention capacity, which is resulting for the combined effect of the high surface-to-volume ratio and hydrophilic nature of pAsp, could potentially find applications in the biomedical and cosmetics field [51]. The fibrous networks could for example be developed to serve as wound dressings, to take up excessive wound exudate or to deliver therapeutic agents [39,55], or as hydration skin care masks, as they can retain and release moisture to hydrate and potentially transfer additives to the skin [63]. Furthermore, electrospun hydrogel networks based on biomaterials, have been used in tissue engineering applications to prepare artificial matrices to mimic living tissue [20,52,80]. However, for these applications, extensive biocompatibility and cytotoxicity assays are required, given the envisioned contact with the skin or other living tissue. Another potential use of the fibrous hydrogel networks which benefits from the large surface area of electrospun membranes and the anionic nature of pAsp encompasses sensing applications, *e.g.* to detect and adsorb metal ions for wastewater treatment [50].

CRediT authorship contribution statement

Lauren De Grave: Conceptualization, Data curation, Formal analysis, Investigation, Methodology, Software, Validation, Visualization, Writing – original draft, Writing – review & editing. **Katrien V. Bernaerts:** Conceptualization, Funding acquisition, Project administration, Supervision, Validation, Writing – review & editing. **Sandra Van Vlierberghe:** Conceptualization, Funding acquisition, Project administration, Resources, Supervision, Validation, Writing – review & editing.

Declaration of Competing Interest

The authors declare that they have no known competing financial interests or personal relationships that could have appeared to influence the work reported in this paper.

Data Availability

Data will be made available on request.

Acknowledgements

Project ‘GREENER’ was financed within the Interreg V program Flanders-the Netherlands, a cross-border consortium with financial support of the European Fund for Regional Development with co-financing of the province East-Flanders and the Ministry of Economic Affairs and Climate (the Netherlands). The authors would further like to acknowledge Sofiya Vynnytska for the GPC measurements, Lobke De Vos and Astrid Quaak for the XPS measurements and Kristyna Kolouchova for acquiring the SEM pictures. The authors also want to thank the NMR expertise center (Ghent University) for providing access to its NMR infrastructure.

Appendix A. Supporting information

Supplementary data associated with this article can be found in the online version at doi:10.1016/j.nxmate.2024.100172.

References

[1] J.-S. Park, Electrospinning and its applications, Adv. Nat. Sci. Nanosci. Nanotechnol. 1 (2011) 043002, https://doi.org/10.1088/2043-6262/1/4/043002.
[2] J. Xue, T. Wu, Y. Dai, Y. Xia, Electrospinning and electrospun nanofibers: methods, materials, and applications, Chem. Rev. 119 (2019) 5298–5415, https://doi.org/10.1021/acs.chemrev.8b00593.
[3] N. Bhardwaj, S.C. Kundu, Electrospinning: a fascinating fiber fabrication technique, Biotechnol. Adv. 28 (2010) 325–347, https://doi.org/10.1016/j.biotechadv.2010.01.004.
[4] H.M. Ibrahim, A. Klingner, A review on electrospun polymeric nanofibers: production parameters and potential applications, Polym. Test. 90 (2020) 106647, https://doi.org/10.1016/j.polymertesting.2020.106647.
[5] T.U. Rashid, R.E. Gorga, W.E. Krause, Mechanical properties of electrospun fibers—a critical review, Adv. Eng. Mater. 23 (2021) 2100153, https://doi.org/10.1002/adem.202100153.
[6] L. Zhao, G. Duan, G. Zhang, H. Yang, S. He, S. Jiang, Electrospun functional materials toward food packaging applications: a review, Nanomaterials 10 (2020) 150, https://doi.org/10.3390/nano10010150.
[7] X. Li, W. Chen, Q. Qian, H. Huang, Y. Chen, Z. Wang, Q. Chen, J. Yang, J. Li, Y. Mai, Electrospinning-based strategies for battery materials, Adv. Energy Mater. 11 (2021) 2000845, https://doi.org/10.1002/aenm.202000845.
[8] Z. Dong, S.J. Kennedy, Y. Wu, Electrospinning materials for energy-related applications and devices, J. Power Sources 196 (2011) 4886–4904, https://doi.org/10.1016/j.jpowsour.2011.01.090.
[9] S. Chattopadhyay, T.A. Hatton, G.C. Rutledge, Aerosol filtration using electrospun cellulose acetate fibers, J. Mater. Sci. 51 (2016) 204–217, https://doi.org/10.1007/s10853-015-9286-4.
[10] A. Luraghi, F. Peri, L. Moroni, Electrospinning for drug delivery applications: a review, J. Control. Release 334 (2021) 463–484, https://doi.org/10.1016/j.jconrel.2021.03.033.
[11] J. Venugopal, M. Prabhakaran, S. Low, A. Choon, G. Deepika, V. Giri Dev, S. Ramakrishna, Continuous nanostructures for the controlled release of drugs, Curr. Pharm. Des. 15 (2009) 1799–1808, https://doi.org/10.2174/138161209788186344.

[12] J. Varshosaz, M. Jannesari, M. Morshed, M. Zamani, Composite poly(vinyl alcohol)/poly(vinyl acetate) electrospun nanofibrous mats as a novel wound dressing matrix for controlled release of drugs, Int. J. Nanomed. 6 (2011) 993–1003, https://doi.org/10.2147/IJN.S17595.
[13] O.M. Ionescu, A. Mignon, M. Minsart, I.-D. Caruntu, S.E. Giusca, I. Gardikiotis, S. Van Vlierberghe, L. Profire, Acrylate-endcapped urethane-based hydrogels: an in vivo study on wound healing potential, Mater. Sci. Eng. C. 130 (2021) 112436, https://doi.org/10.1016/j.msec.2021.112436.
[14] S.D. McCullen, S. Ramaswamy, L.I. Clarke, R.E. Gorga, Nanofibrous composites for tissue engineering applications, WIREs Nanomed. Nanobiotechnol. 1 (2009) 369–390, https://doi.org/10.1002/wnan.39.
[15] M. Rahmati, D.K. Mills, A.M. Urbanska, M.R. Saeb, J.R. Venugopal, S. Ramakrishna, M. Mozafari, Electrospinning for tissue engineering applications, Prog. Mater. Sci. 117 (2021) 100721, https://doi.org/10.1016/j.pmatsci.2020.100721.
[16] N. Pien, S. Palladino, F. Copes, G. Candiani, P. Dubruel, S. Van Vlierberghe, D. Mantovani, Tubular bioartificial organs: from physiological requirements to fabrication processes and resulting properties. a critical review, Cells Tissues Organs 211 (2022) 420–446, https://doi.org/10.1159/000519207.
[17] N. Pien, H. Krzyslak, S. Shastry Kallaje, J. Van Meerssche, D. Mantovani, C. De Schauwer, P. Dubruel, S. Van Vlierberghe, C.P. Pennisi, Tissue engineering of skeletal muscle, tendons and nerves: a review of manufacturing strategies to meet structural and functional requirements, Appl. Mater. Today 31 (2023) 101737, https://doi.org/10.1016/j.apmt.2023.101737.
[18] K. Molnar, B. Jozsa, D. Barczikai, E. Krisch, J.E. Puskas, A. Jedlovszky-Hajdu, Plasma treatment as an effective tool for crosslinking of electrospun fibers, J. Mol. Liq. 303 (2020) 112628, https://doi.org/10.1016/j.molliq.2020.112628.
[19] S.H. Kim, S.-H. Kim, S. Nair, E. Moore, Reactive electrospinning of cross-linked poly(2-hydroxyethyl methacrylate) nanofibers and elastic properties of individual hydrogel nanofibers in aqueous solutions, Macromolecules 38 (2005) 3719–3723, https://doi.org/10.1021/ma050308g.
[20] K. Molnar, D. Juriga, P.M. Nagy, K. Sinko, A. Jedlovszky-Hajdu, M. Zrinyi, Electrospun poly(aspartic acid) gel scaffolds for artificial extracellular matrix, Polym. Int. 63 (2014) 1608–1615, https://doi.org/10.1002/pi.4720.
[21] K. Molnar, A. Jedlovszky-Hajdu, M. Zrinyi, S. Jiang, S. Agarwal, Poly(amino acid)-based gel fibers with ph responsivity by coaxial reactive electrospinning, Macromol. Rapid Commun. 38 (2017) 1700147, https://doi.org/10.1002/marc.201700147.
[22] A. Houben, P. Roose, H. Van den Bergen, H. Declercq, J. Van Hoorick, P. Gruber, A. Ovsianikov, D. Bontinck, S. Van Vlierberghe, P. Dubruel, Flexible oligomer spacers as the key to solid-state photopolymerization of hydrogel precursors, Mater. Today Chem. 4 (2017) 84–89, https://doi.org/10.1016/j.mtchem.2017.01.005.
[23] J. Zeng, H. Hou, J.H. Wendorff, A. Greiner, Photo-induced solid-state crosslinking of electrospun poly(vinyl alcohol) fibers, Macromol. Rapid Commun. 26 (2005) 1557–1562, https://doi.org/10.1002/marc.200500545.
[24] Y.-J. Kim, M. Ebara, T. Aoyagi, Temperature-responsive electrospun nanofibers for 'on–off' switchable release of dextran, Sci. Technol. Adv. Mater. 13 (2012) 064203, https://doi.org/10.1088/1468-6996/13/6/064203.
[25] B.L. Dargaville, C. Vaquette, F. Rasoul, J.J. Cooper-White, J.H. Campbell, A. K. Whittaker, Electrospinning and crosslinking of low-molecular-weight poly (trimethylene carbonate-co-l-lactide) as an elastomeric scaffold for vascular engineering, Acta Biomater. 9 (2013) 6885–6897, https://doi.org/10.1016/j.actbio.2013.02.009.
[26] K.H. Sizeland, K.A. Hofman, I.C. Hallett, D.E. Martin, J. Potgieter, N.M. Kirby, A. Hawley, S.T. Mudie, T.M. Ryan, R.G. Haverkamp, M.H. Cumming, Nanostructure of electrospun collagen: do electrospun collagen fibers form native structures? Materialia 3 (2018) 90–96, https://doi.org/10.1016/j.mtla.2018.10.001.
[27] I. Steyaert, H. Rahier, S. Van Vlierberghe, J. Olijve, K. De Clerck, Gelatin nanofibers: analysis of triple helix dissociation temperature and cold-water-solubility, Food Hydrocoll. 57 (2016) 200–208, https://doi.org/10.1016/j.foodhyd.2016.01.016.
[28] M. Skotak, S. Noriega, G. Larsen, A. Subramanian, Electrospun cross-linked gelatin fibers with controlled diameter: the effect of matrix stiffness on proliferative and biosynthetic activity of chondrocytes cultured in vitro, J. Biomed. Mater. Res. Part A. 95A (2010) 828–836, https://doi.org/10.1002/jbm.a.32850.
[29] M. Minsart, A. Mignon, A. Arslan, I.U. Allan, S. Van Vlierberghe, P. Dubruel, Activated carbon containing PEG-based hydrogels as novel candidate dressings for the treatment of malodorous wounds, Macromol. Mater. Eng. 306 (2021) 2000529, https://doi.org/10.1002/mame.202000529.
[30] B. Stubbe, Y. Li, M. Vergaelen, S. Van Vlierberghe, P. Dubruel, K. De Clerck, R. Hoogenboom, Aqueous electrospinning of poly(2-ethyl-2-oxazoline): mapping the parameter space, Eur. Polym. J. 88 (2017) 724–732, https://doi.org/10.1016/j.eurpolymj.2016.09.014.
[31] O.I. Kalaoglu-Altan, Y. Li, R. McMaster, A. Shaw, Z. Hou, M. Vergaelen, R. Hoogenboom, T.R. Dargaville, K. De Clerck, Crosslinking of electrospun and bioextruded partially hydrolyzed poly(2-ethyl-2-oxazoline) using glutaraldehyde vapour, Eur. Polym. J. 120 (2019) 109218, https://doi.org/10.1016/j.eurpolymj.2019.109218.
[32] N. Pien, Y. Van de Maele, L. Parmentier, M. Meeremans, A. Mignon, C. De Schauwer, I. Peeters, L. De Wilde, A. Martens, D. Mantovani, S. Van Vlierberghe, P. Dubruel, Design of an electrospun tubular construct combining a mechanical and biological approach to improve tendon repair, J. Mater. Sci. Mater. Med. 33 (2022) 51, https://doi.org/10.1007/s10856-022-06673-4.
[33] N. Pien, I. Peeters, L. Deconinck, L. Van Damme, L. De Wilde, A. Martens, S. Van Vlierberghe, P. Dubruel, A. Mignon, Design and development of a reinforced tubular electrospun construct for the repair of ruptures of deep flexor tendons, Mater. Sci. Eng. C. 119 (2021) 111504, https://doi.org/10.1016/j.msec.2020.111504.
[34] B. Kim, H. Park, S.-H. Lee, W.M. Sigmund, Poly(acrylic acid) nanofibers by electrospinning, Mater. Lett. 59 (2005) 829–832, https://doi.org/10.1016/j.matlet.2004.11.032.
[35] W. Han, L. Wang, Q. Li, B. Ma, C. He, X. Guo, J. Nie, G. Ma, A review: current status and emerging developments on natural polymer-based electrospun fibers, Macromol. Rapid Commun. 43 (2022), https://doi.org/10.1002/marc.202200456.
[36] S. Nemati Mahand, S. Aliakbarzadeh, A. Moghaddam, A. Salehi Moghaddam, B. Kruppke, M. Nasrollahzadeh, H.A. Khonakdar, Polyoxazoline: a review article from polymerization to smart behaviors and biomedical applications, Eur. Polym. J. 178 (2022) 111484, https://doi.org/10.1016/j.eurpolymj.2022.111484.
[37] G. Dalei, S. Das, Polyacrylic acid-based drug delivery systems: a comprehensive review on the state-of-art, J. Drug Deliv. Sci. Technol. 78 (2022) 103988, https://doi.org/10.1016/j.jddst.2022.103988.
[38] K. Devarayan, S. Nakagami, S. Suzuki, I. Yuki, K. Ohkawa, Electrospinning and post-spun chain conformations of synthetic, hydrophobic poly(α-amino acid)s, Polym. (Basel) 12 (2020) 327, https://doi.org/10.3390/polym12020327.
[39] Y. Ji, W. Song, L. Xu, D.-G. Yu, S.W. Annie Bligh, A review on electrospun poly (amino acid) nanofibers and their applications of hemostasis and wound healing, Biomolecules 12 (2022) 794, https://doi.org/10.3390/biom12060794.
[40] S.S. Gupta, V. Mishra, M.Das Mukherjee, P. Saini, K.R. Ranjan, Amino acid derived biopolymers: recent advances and biomedical applications, Int. J. Biol. Macromol. 188 (2021) 542–567, https://doi.org/10.1016/j.ijbiomac.2021.08.036.
[41] D.D. Alford, A.P. Wheeler, C.A. Pettigrew, Biodegradation of thermally synthesized polyaspartate, J. Environ. Polym. Degrad. 2 (1994) 225–236, https://doi.org/10.1007/BF02071970.
[42] H. Adelnia, H.D.N. Tran, P.J. Little, I. Blakey, H.T. Ta, Poly(aspartic acid) in biomedical applications: from polymerization, modification, properties, degradation, and biocompatibility to applications, ACS Biomater. Sci. Eng. 7 (2021) 2083–2105, https://doi.org/10.1021/acsbiomaterials.1c00150.
[43] H. Adelnia, I. Blakey, P.J. Little, H.T. Ta, Hydrogels based on poly(aspartic acid): synthesis and applications, Front. Chem. 7 (2019), https://doi.org/10.3389/fchem.2019.00755.
[44] E. Jalalvandi, A. Shavandi, Polysuccinimide and its derivatives: degradable and water soluble polymers (review), Eur. Polym. J. 109 (2018) 43–54, https://doi.org/10.1016/j.eurpolymj.2018.08.056.
[45] C. Németh, B. Gyarmati, J. Gacs, D.V. Salakhieva, K. Molnár, T. Abdullin, K. László, A. Szilágyi, Fast dissolving nanofibrous matrices prepared by electrospinning of polyaspartamides, Eur. Polym. J. 130 (2020) 109624, https://doi.org/10.1016/j.eurpolymj.2020.109624.
[46] K. Tóth, K. S. Nagy, Z. Güler, Á.G. Juhász, É. Pállinger, G. Varga, A.S. Sarac, M. Zrínyi, A. Jedlovszky-Hajdú, D. Juriga, Characterization of Electrospun Polysuccinimide-Dopamine Conjugates and Effect on Cell Viability and Uptake, Macromol. Biosci. 23 (2023) 2200397, https://doi.org/10.1002/mabi.202200397.
[47] D. Barczikai, V. Kacsari, J. Domokos, D. Szabó, A. Jedlovszky-Hajdu, Interaction of silver nanoparticle and commonly used anti-inflammatory drug within a poly (amino acid) derivative fibrous mesh, J. Mol. Liq. 322 (2021) 114575, https://doi.org/10.1016/j.molliq.2020.114575.
[48] K. Molnar, C. Voniatis, D. Feher, G. Szabo, R. Varga, L. Reiniger, D. Juriga, Z. Kiss, E. Krisch, G. Weber, A. Ferencz, G. Varga, M. Zrinyi, K.S. Nagy, A. Jedlovszky-Hajdu, Poly(amino acid) based fibrous membranes with tuneable in vivo biodegradation, PLoS One 16 (2021) e0254843, https://doi.org/10.1371/journal.pone.0254843.
[49] C. Zhang, L.Y. Wan, S. Wu, D. Wu, X. Qin, F. Ko, A reversible colorimetric chemosensor for naked-eye detection of copper ions using poly (aspartic acid) nanofibrous hydrogel, Dye. Pigment. 123 (2015) 380–385, https://doi.org/10.1016/j.dyepig.2015.07.028.
[50] C. Zhang, H. Li, Q. Yu, L. Jia, L.Y. Wan, Poly(aspartic acid) electrospun nanofiber hydrogel membrane-based reusable colorimetric sensor for Cu(II) and Fe(III) detection, ACS Omega 4 (2019) 14633–14639, https://doi.org/10.1021/acsomega.9b02109.
[51] M.S. Islam, B.C. Ang, A. Andriyana, A.M. Afifi, A review on fabrication of nanofibers via electrospinning and their applications, SN Appl. Sci. 1 (2019) 1248, https://doi.org/10.1007/s42452-019-1288-4.
[52] T.J. Sill, H.A. von Recum, Electrospinning: applications in drug delivery and tissue engineering, Biomaterials 29 (2008) 1989–2006, https://doi.org/10.1016/j.biomaterials.2008.01.011.
[53] R. Bucci, E. Georgilis, A.M. Bittner, M.L. Gelmi, F. Clerici, Peptide-based electrospun fibers: current status and emerging developments, Nanomaterials 11 (2021) 1262, https://doi.org/10.3390/nano11051262.
[54] K. Halicka, J. Cabaj, Electrospun nanofibers for sensing and biosensing applications—A review, Int. J. Mol. Sci. 22 (2021) 6357, https://doi.org/10.3390/ijms22126357.
[55] Y. Liu, T. Li, Y. Han, F. Li, Y. Liu, Recent development of electrospun wound dressing, Curr. Opin. Biomed. Eng. 17 (2021) 100247, https://doi.org/10.1016/j.cobme.2020.100247.
[56] M.B. Stie, K. Kalouta, C.F.B. da Cunha, H.M. Feroze, V. Vetri, V. Foderà, Sustainable strategies for waterborne electrospinning of biocompatible nanofibers based on soy protein isolate, Sustain. Mater. Technol. 34 (2022) e00519, https://doi.org/10.1016/j.susmat.2022.e00519.
[57] A. Jedlovszky-Hajdu, K. Molnar, P.M. Nagy, K. Sinko, M. Zrínyi, Preparation and properties of a magnetic field responsive three-dimensional electrospun polymer

scaffold, Colloids Surf. A Physicochem. Eng. Asp. 503 (2016) 79–87, https://doi.org/10.1016/j.colsurfa.2016.05.036.
[58] C. Zhang, S. Wu, X. Qin, Facile fabrication of novel pH-sensitive poly(aspartic acid) hydrogel by crosslinking nanofibers, Mater. Lett. 132 (2014) 393–396, https://doi.org/10.1016/j.matlet.2014.06.031.
[59] C. Zhang, S. Wu, J. Wu, D. Wu, X. Qin, Preparation and characterization of microporous sodium poly(aspartic acid) nanofibrous hydrogel, J. Porous Mater. 24 (2017) 75–84, https://doi.org/10.1007/s10934-016-0239-3.
[60] R. Pázmány, K.S. Nagy, Á. Zsembery, A. Jedlovszky–Hajdu, Ultrasound induced, easy-to-store porous poly(amino acid) based electrospun scaffolds, J. Mol. Liq. 359 (2022) 119243, https://doi.org/10.1016/j.molliq.2022.119243.
[61] L. De Grave, J.R. Tenório Filho, D. Snoeck, S. Vynnytska, N. De Belie, K. V. Bernaerts, S. Van Vlierberghe, Poly(aspartic acid) superabsorbent polymers as biobased and biodegradable additives for self-sealing of cementitious mortar, J. Sustain. Cem. Mater. 12 (2023) 925–940, https://doi.org/10.1080/21650373.2022.2137861.
[62] L. De Grave, C. Di Meo, C. Gréant, B. Van Durme, M. Gérard, A. La Gatta, C. Schiraldi, L. Thorrez, K.V. Bernaerts, S. Van Vlierberghe, Photo-crosslinkable Poly(aspartic acid) for Light-based additive Manufacturing: chain-growth versus Step-growth crosslinking, Eur. Polym. J. 190 (2023) 112017, https://doi.org/10.1016/j.eurpolymj.2023.112017.
[63] Z.-M. Huang, Y.-Z. Zhang, M. Kotaki, S. Ramakrishna, A review on polymer nanofibers by electrospinning and their applications in nanocomposites, Compos. Sci. Technol. 63 (2003) 2223–2253, https://doi.org/10.1016/S0266-3538(03)00178-7.
[64] J. Anu Bhushani, C. Anandharamakrishnan, Electrospinning and electrospraying techniques: Potential food based applications, Trends Food Sci. Technol. 38 (2014) 21–33, https://doi.org/10.1016/j.tifs.2014.03.004.
[65] J. Wang, J.A. Jansen, F. Yang, Electrospraying: Possibilities and challenges of engineering carriers for biomedical applications—A mini review, Front. Chem. 7 (2019), https://doi.org/10.3389/fchem.2019.00258.
[66] J. Guerrero, J. Rivero, V.R. Gundabala, M. Perez-Saborid, A. Fernandez-Nieves, Whipping of electrified liquid jets, Proc. Natl. Acad. Sci. 111 (2014) 13763–13767, https://doi.org/10.1073/pnas.1411698111.
[67] S.L. Shenoy, W.D. Bates, H.L. Frisch, G.E. Wnek, Role of chain entanglements on fiber formation during electrospinning of polymer solutions: good solvent, non-specific polymer–polymer interaction limit, Polym. (Guildf.) 46 (2005) 3372–3384, https://doi.org/10.1016/j.polymer.2005.03.011.
[68] S. Zargham, S. Bazgir, A. Tavakoli, A.S. Rashidi, R. Damerchely, The Effect of Flow Rate on Morphology and Deposition Area of Electrospun Nylon 6 Nanofiber, 155892501200700, J. Eng. Fiber Fabr. 7 (2012), https://doi.org/10.1177/155892501200700414.
[69] C.J. Thompson, G.G. Chase, A.L. Yarin, D.H. Reneker, Effects of parameters on nanofiber diameter determined from electrospinning model, Polym. (Guildf.) 48 (2007) 6913–6922, https://doi.org/10.1016/j.polymer.2007.09.017.
[70] Y. Duan, L. Kalluri, M. Satpathy, Y. Duan, Effect of Electrospinning parameters on the fiber diameter and morphology of PLGA nanofibers, Dent. Oral. Biol. Craniofacial Res. (2021) 1–7, https://doi.org/10.31487/j.DOBCR.2021.02.04.
[71] A. Refate, Y. Mohamed, M. Mohamed, M. Sobhy, K. Samhy, O. Khaled, K. Eidaroos, H. Batikh, E. El-Kashif, S. El-Khatib, S. Mehanny, Influence of electrospinning parameters on biopolymers nanofibers, with emphasis on cellulose & chitosan, Heliyon 9 (2023) e17051, https://doi.org/10.1016/j.heliyon.2023.e17051.
[72] S. Hofmann, Practical surface analysis: state of the art and recent developments in AES, XPS, ISS and SIMS, Surf. Interface Anal. 9 (1986) 3–20, https://doi.org/10.1002/sia.740090104.
[73] R.M. Smith, D.E. Hansen, The pH-Rate Profile for the Hydrolysis of a Peptide Bond, J. Am. Chem. Soc. 120 (1998) 8910–8913, https://doi.org/10.1021/ja9804565.
[74] E.M. Jeffries, R.A. Allen, J. Gao, M. Pesce, Y. Wang, Highly elastic and suturable electrospun poly(glycerol sebacate) fibrous scaffolds, Acta Biomater. 18 (2015) 30–39, https://doi.org/10.1016/j.actbio.2015.02.005.
[75] F. Xu, H. Sheardown, T. Hoare, Reactive electrospinning of degradable poly (oligoethylene glycol methacrylate)-based nanofibrous hydrogel networks, Chem. Commun. 52 (2016) 1451–1454, https://doi.org/10.1039/C5CC08053C.
[76] A. Liguori, A. Bigi, V. Colombo, M.L. Focarete, M. Gherardi, C. Gualandi, M. C. Oleari, S. Panzavolta, Atmospheric pressure non-equilibrium plasma as a green tool to crosslink gelatin nanofibers, Sci. Rep. 6 (2016) 38542, https://doi.org/10.1038/srep38542.
[77] S. Khan, N.M. Ranjha, Effect of degree of cross-linking on swelling and on drug release of low viscous chitosan/poly(vinyl alcohol) hydrogels, Polym. Bull. 71 (2014) 2133–2158, https://doi.org/10.1007/s00289-014-1178-2.
[78] Á.G. Juhász, M. Nanys, B. Pinke, A. Fadel, M. Godzierz, K. Juriga-Tóth, K. Molnár, D. Juriga, A. Jedlovszky-Hajdú, Formation of three-dimensional polysuccinimide electrospun fiber meshes induced by the combination of CaCl 2 and humidity, Macromol. Rapid Commun. (2024), https://doi.org/10.1002/marc.202300625.
[79] Y. Li, J. Wang, Y. Wang, W. Cui, Advanced electrospun hydrogel fibers for wound healing, Compos. Part B Eng. 223 (2021) 109101, https://doi.org/10.1016/j.compositesb.2021.109101.
[80] B.-S. Kim, I.-K. Park, T. Hoshiba, H.-L. Jiang, Y.-J. Choi, T. Akaike, C.-S. Cho, Design of artificial extracellular matrices for tissue engineering, Prog. Polym. Sci. 36 (2011) 238–268, https://doi.org/10.1016/j.progpolymsci.2010.10.001.